

Organic aerosol formation from 222 nm germicidal light: ozone-initiated vs. non-ozone pathways

Matthew B. Goss¹ and Jesse H. Kroll^{1,2}

¹Department of Civil and Environmental Engineering, Massachusetts Institute of Technology, Cambridge, Massachusetts 02139, United States

²Department of Chemical Engineering, Massachusetts Institute of Technology, Cambridge, Massachusetts 02139, United States

Abstract

Germicidal ultraviolet lamps outputting 222 nm light (GUV₂₂₂) have the potential to reduce the airborne spread of disease through effective inactivation of pathogens, while remaining safe for direct human exposure. However, recent studies have identified these lamps as a source of ozone and other secondary pollutants such as secondary organic aerosol (SOA), and the health effects of these pollutants must be balanced against the benefits of pathogen inactivation. While ozone reactions are likely to account for much of this secondary indoor air pollution, 222 nm light may initiate additional non-ozone chemical processes, including the formation of other oxidants and direct photolytic reactions, which are not as well understood. This work examines the impacts of GUV₂₂₂ light on SOA formation and composition by comparing limonene oxidation under GUV₂₂₂ and O₃-only control conditions in a laboratory chamber. Differences between these experiments enable us to distinguish patterns in aerosol formation driven by ozone chemistry from those driven by other photolytic processes. These experiments also examine the influence of the addition of NO₂ and nitrous acid (HONO), and investigate SOA formation in sampled outdoor air. SOA composition and yield vary only slightly with respect to GUV₂₂₂ vs ozone-only conditions; NO₂ and HONO photolysis do not appreciably affect the observed chemistry. In contrast, we observe consistent new particle formation under high-fluence 222 nm light (45 μW cm⁻²) that differs dramatically from ozone-only experiments. This observed new particle formation represents an additional reason to keep GUV₂₂₂ fluence rates to the lowest effective levels.

Environmental Significance Statement

Germicidal ultraviolet lamps that emit light at 222 nm (GUV₂₂₂) can be a useful tool for reducing the airborne spread of disease in indoor environments, but might also negatively impact indoor air quality through the formation of ozone and particulate matter. This work demonstrates that GUV₂₂₂ lamps not only drive increases in total particulate mass due to reactions of ozone with organic species, but also increase new particle formation in excess of what is caused by such reactions. The formation of ultrafine aerosol particles represents a potential health hazard in the indoor environment, and GUV₂₂₂ applications should therefore keep fluence rates to the minimum effective levels to reduce negative impacts to indoor air quality.

37 Introduction

38 The COVID-19 pandemic has increased interest in germicidal ultraviolet (GUV) light as
39 a potential strategy for reducing the airborne spread of disease. Traditional applications of GUV
40 light have used 254 nm mercury lamps, which effectively inactivate airborne pathogens, but pose
41 a threat to human health if shined directly on skin and eyes. Newly available filtered KrCl
42 excimer lamps, which emit light at 222 nm, have been reported to efficiently inactivate
43 pathogens while still being safe for direct human exposure.^{1,2} Due to its shorter wavelength, the
44 light does not penetrate the top layer of the skin or ocular tear layer, minimizing concerns about
45 human ultraviolet light exposure.^{3,4}

46 However, recent work has raised concerns about the effects of 222 nm light (GUV₂₂₂) on
47 indoor air quality,⁵⁻¹¹ in large part due to the production of ozone, a well-known human health
48 hazard.^{12,13} Ozone production from GUV₂₂₂, proceeding through the photolysis of O₂ followed
49 by the reaction of the resulting O atoms with O₂ to form O₃, is now well documented through
50 both modeling calculations and laboratory experiments.⁵⁻⁸ Under laboratory conditions, GUV₂₂₂
51 irradiation can lead to high (> 100 ppb) O₃ levels, but in real indoor spaces, O₃ increases are
52 generally much lower (~6.5 ppb increase observed in an office,⁷ ~5 ppb increase in a restroom¹¹)
53 due to the loss of ozone to indoor surfaces and relatively low average GUV₂₂₂ fluence rates.
54 These modest increases represent a potential source of concern given that the integrated exposure
55 to indoor ozone is magnified by the amount of time people spend indoors;¹⁴ associated increases
56 in oxidized volatile organic compounds (OVOCs) compound this potential hazard.^{11,15}

57 While some prior studies have primarily focused on quantifying ozone production from
58 GUV₂₂₂,^{5,7} 222 nm light has the potential to drive chemistry beyond O₂ photolysis. As
59 demonstrated in previous work,^{6,8,9} GUV₂₂₂ can form the hydroxyl radical (OH), both through
60 ozone photolysis and through the reaction of ozone with alkenes. Ozone and OH both react with
61 volatile organic compounds, resulting in the production of OVOCs and secondary organic
62 aerosol (SOA) particles.^{8,9,11} Previous work has also identified GUV₂₂₂-driven new particle
63 formation under some conditions,^{8,11,16} which could act as a source of ultrafine particles in the
64 indoor environment. Finally, a recent field study has characterized SOA formation and growth in
65 the presence of GUV₂₂₂ in a typical indoor space,¹¹ demonstrating that these products of
66 secondary chemistry, particularly SOA, can be formed under real-world conditions.

67 While this previous work has examined the formation of secondary pollutants other than
68 ozone, the extent to which photochemical processes that do not directly involve ozone (referred
69 to here as “non-ozone chemistry”) affect secondary chemistry and aerosol formation is unclear.
70 Previous work^{8,9,11} demonstrates that SOA forms in the presence of GUV₂₂₂, but less is known
71 about the effects of GUV₂₂₂ light on SOA yield and composition, relative to SOA formed solely
72 from reactions with ozone. Further, new particle formation sometimes observed under 222 nm
73 light is not understood. In addition, in our previous work,⁸ we suggested that the photolysis of
74 other species, such as NO₂, HONO, and photolabile organic molecules, may affect OH
75 concentrations or radical cycling, but to our knowledge, such photolytic processes have not yet
76 been explored.

77 The present work seeks to better understand non-ozone chemistry stemming from
78 GUV₂₂₂ irradiation, specifically focusing on secondary organic aerosol formation, and the
79 potential role of trace species that can be present in indoor air. Experiments compare aerosol
80 formation under 222 nm light and O₃-only control conditions to identify differences driven by
81 photolysis; these may be direct, for example by photolysis of an organic species, or indirect, for
82 example from chemistry initiated by photolytically-formed OH. Using limonene as a model
83 compound, chosen because of its common use in household cleaning products and propensity to
84 generate SOA,¹⁷ we perform a series of experiments in two environmental chambers to identify
85 differences in aerosol yield, composition, and tendency to form new particles. While this study
86 does not seek to directly mimic indoor conditions (e.g., we do not include reactive surfaces), we
87 also investigate more complex indoor mixtures by examining the influence of NO_x and HONO,
88 often present in moderate concentrations in indoor spaces,^{18,19} on GUV₂₂₂-derived aerosol
89 production, and by performing experiments in which clean laboratory air is replaced by ambient
90 outdoor air. This work focuses on the chemical processes stemming from 222 nm irradiation, and
91 as such uses higher GUV₂₂₂ fluence rates and VOC concentrations than are typically found in
92 indoor environments, in order to enhance the distinctions between 222 nm and O₃-only
93 chemistry.

94 **Methods**

95 Experiments are carried out in two differently-sized Teflon chambers, described
96 previously.^{8,20,21} The first (7.5 m³ in volume, referred to as the “large chamber”) is characterized
97 by a relatively low particle wall loss rate and low GUV₂₂₂ fluence rate, and is primarily used to
98 quantify aerosol yield. The second one (0.15 m³ volume, referred to as the “mini chamber”) is
99 used to study aerosol composition and size distribution trends due to its shorter residence time
100 that more easily enables replicates. Both chambers are operated in “semi-batch mode,” in which
101 clean air is continuously introduced to maintain slight positive pressure and make up for air
102 removed through sampling.

103 All experiments compare the effects of GUV₂₂₂ with ozone-only conditions by matching
104 ozone concentrations in the chamber for each experiment. For “GUV₂₂₂” experiments, ozone is
105 produced by the GUV₂₂₂ lamp (Ushio, Care222 B1 Illuminator, peak emission at 222 nm).
106 Average GUV₂₂₂ fluence rate is estimated to be 45 μW cm⁻² for the mini chamber⁸ and 3.9 μW
107 cm⁻² for the large chamber (see SI). For “ozone-only” experiments, the lamp is kept off and
108 ozone is produced using an ozone generator (Jelight Model 610); ozone generation is tuned to
109 match production by the GUV₂₂₂ lamp by adjusting the lamp sleeve and reducing the power
110 delivered using a Variac. Experiments are alternated between GUV₂₂₂ and ozone-only conditions
111 to avoid systematic biases in chamber conditions.

112 Materials and methods are broadly the same for both large (n = 7) and small chamber
113 experiments (n = 33). Clean air used for flushing and dilution for limonene oxidation
114 experiments was produced by a zero-air generator (AADCO Model 737) (expts. 1 – 13) or
115 supplied from an ultra zero air tank (Linde) (expts. 15 – 32). Relative humidity for dry (<1%
116 RH) or humid (27 – 45% RH) experiments is adjusted by bubbling an additional flow of clean air
117 through Milli-Q water. Most experiments use (*R*)-(+)-limonene (C₁₀H₁₆, Sigma Aldrich) as a

118 precursor VOC, ammonium sulfate ((NH₄)₂SO₄, Sigma Aldrich) for aerosol seed particles, and
119 hexafluorobenzene (C₆F₆, Sigma Aldrich) as a dilution tracer. Specific details for each
120 experiment are provided in Tables S1 and S2, and more detailed experimental methods are
121 included in section S.2.

122 Mini chamber experiments are carried out in two sets, separated by approximately 5
123 months; we refer to the earlier and later sets by the year they were carried out (2023 or 2024).
124 For each mini chamber experiment, total dilution flows are maintained at 10.5 LPM, resulting in
125 a measured dilution rate of 2.7 air changes per hour (ACH) (2023 experiments) or 3.2 ACH
126 (2024 experiments) (these differ due to a small leak in the bubbler used in the 2023 experiments).
127 Ozone is first allowed to reach a steady-state concentration (for NO_x-free experiments: 106 ± 6
128 ppb (1σ)) by turning on the ozone generator or the GUV₂₂₂ lamp, mounted above the chamber as
129 in Barber et al.⁸ Once steady-state ozone is reached, a solution of ammonium sulfate (2 g/L) is
130 atomized into the chamber using an aerosol generator (TSI model 3076). This is followed by the
131 addition of hexafluorobenzene (0.05 μL, 70 ppb), and subsequently limonene (0.1 μL, 100 ppb),
132 initiating the experiment. This timepoint is considered t = 0. For six mini chamber experiments
133 (expts. 27 – 32), an additional flow of NO is added resulting in a steady-state NO_x concentration
134 of 18.2 ± 0.7 ppb (1σ). For another six mini chamber experiments (expts. 35 – 40), outdoor air is
135 used instead of clean air, and is continuously pumped through a stainless steel 0.5 μm filter into
136 the chamber; no VOC, dilution tracer, or aerosol seed are added.

137 For large chamber experiments, total dilution flows are maintained at 20 LPM; measured
138 dilution rate is ~0.16 ACH. The GUV₂₂₂ light is mounted outside the chamber, at the center of
139 one of the square sides. For each experiment, ammonium sulfate (2 g/L) is first atomized into the
140 chamber for 9 minutes. After approximately 30 min, hexafluorobenzene (2.2 μL, 61 ppb) and
141 limonene (6.0 μL, 119 ppb) are sequentially added to the chamber through a coated stainless-
142 steel inlet heated to 50 and 120 °C respectively. The decays of these species are monitored for >
143 1 hr before the start of the experiment. The experiment is initiated by turning on the GUV₂₂₂
144 lamp or the ozone generator (considered t = 0). One large chamber experiment (expt. 7) uses a
145 steady flow of HONO, resulting in a HONO concentration that ranges from 9 to 18 ppb over the
146 course of the experiment (See SI for more details).

147 Particle-phase data are collected using a scanning mobility particle sizer (SMPS, TSI) and
148 an aerosol mass spectrometer (AMS, Aerodyne Research, Inc.²²). For large chamber
149 experiments, AMS data are corrected for dilution and wall losses by normalizing to the
150 ammonium sulfate concentration, and scaled such that initial aerosol seed concentration matches
151 that measured by the SMPS (see SI). Time-dependent aerosol yield is calculated as the mass
152 concentration of organic aerosol divided by the mass concentration of limonene reacted. For mini
153 chamber experiments, AMS data are used primarily for elemental composition analysis;²³ aerosol
154 yields are not calculated due to the uncertainties caused by relatively high particle wall loss rates.
155 New particle formation in limonene mini chamber experiments is quantified by fitting the
156 number-weighted particle size distribution to a linear combination of lognormal distributions at
157 each timestep. For experiments in which no new particle formation occurs, the data are well-
158 represented by a single curve; for experiments in which new particle formation occurs, a second

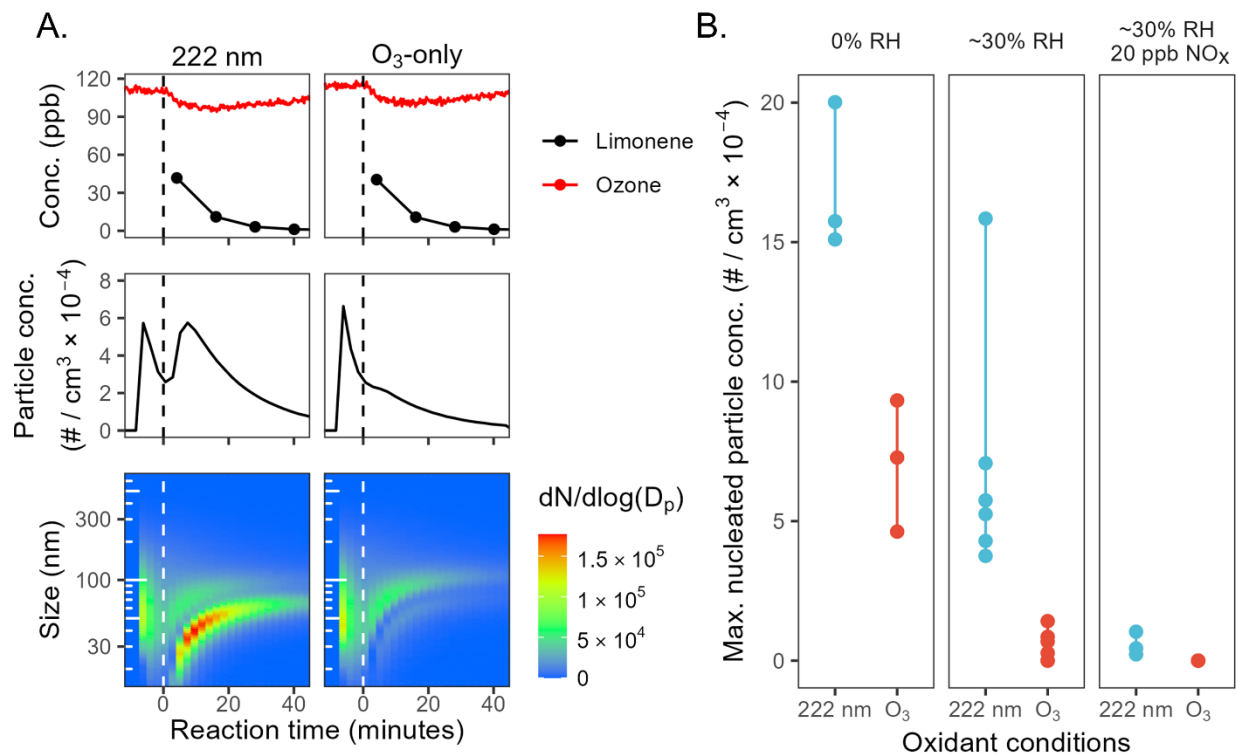
159 mode at smaller particle diameters forms. Where two (or in one case, three) modes are evident,
160 the total particle number associated with the nucleation mode(s) is calculated based on the
161 integral of the lognormal fit; the maximum of this value is considered to be the maximum total
162 new particle formation for purposes of comparing nucleation between experiments. See the SI
163 for further description of this analysis.

164 Gas-phase species are monitored using an additional set of online instrumentation. Ozone
165 concentration is monitored using an ozone monitor (2BTech). Limonene and hexafluorobenzene
166 concentrations are monitored using a gas chromatograph with flame ionization detection (GC-
167 FID, SRI Instruments). For small chamber experiments, the GC-FID is started precisely at $t = 4$
168 min to ensure reproducibility between experiments, since measurements are taken only every 12
169 minutes. For large chamber experiments, limonene concentration is corrected for dilution based
170 on the hexafluorobenzene time series to facilitate the calculation of aerosol yields. In some
171 experiments (see Table S1), trace gas measurements are supplemented with a chemiluminescence
172 NO–NO₂–NO_x analyzer (NO_x analyzer, Thermo Fisher Scientific) and a cavity attenuated phase
173 shift NO₂ monitor (CAPS NO₂, Aerodyne Research, Inc.). The combination of these two
174 instruments allows for quantification of NO, NO₂, and HONO (via subtraction of the CAPS NO₂
175 signal from the NO_x analyzer measurement, see SI). For two sets of experiments, an ammonium
176 chemical ionization mass spectrometer (NH₄⁺ CIMS; modified PTR3²⁴) provides measurements
177 of oxidized gas-phase organic species. While the instrument signal is unstable and uncalibrated
178 during these experiments, it nonetheless provides qualitative insights into gas-phase products.
179 Further instrument details and more complete description of data analysis methods are provided
180 in the supporting information.

181 **Results**

182 *New particle formation*

183 Mini chamber experiments involving limonene oxidation consistently exhibit new
184 particle formation under GUV₂₂₂ irradiation; this is substantially greater than in the ozone-only
185 experiments, often by a large margin. Figure 1A shows results from two consecutive mini-
186 chamber limonene experiments, one with GUV₂₂₂ (expt. 23) and the other with O₃ addition (expt.
187 22). Despite the fact that both have very similar ozone and limonene time series (top panels), far
188 more new particle formation is observed the GUV₂₂₂ case. In the presence of GUV₂₂₂, new
189 particle formation occurs almost immediately after $t = 0$, with total particle number concentration
190 growing to $6 \times 10^4 \text{ cm}^{-3}$. In contrast, the ozone-only experiment exhibits size distribution
191 characteristics of SOA growth on the seed aerosol, with a much smaller nucleation mode.

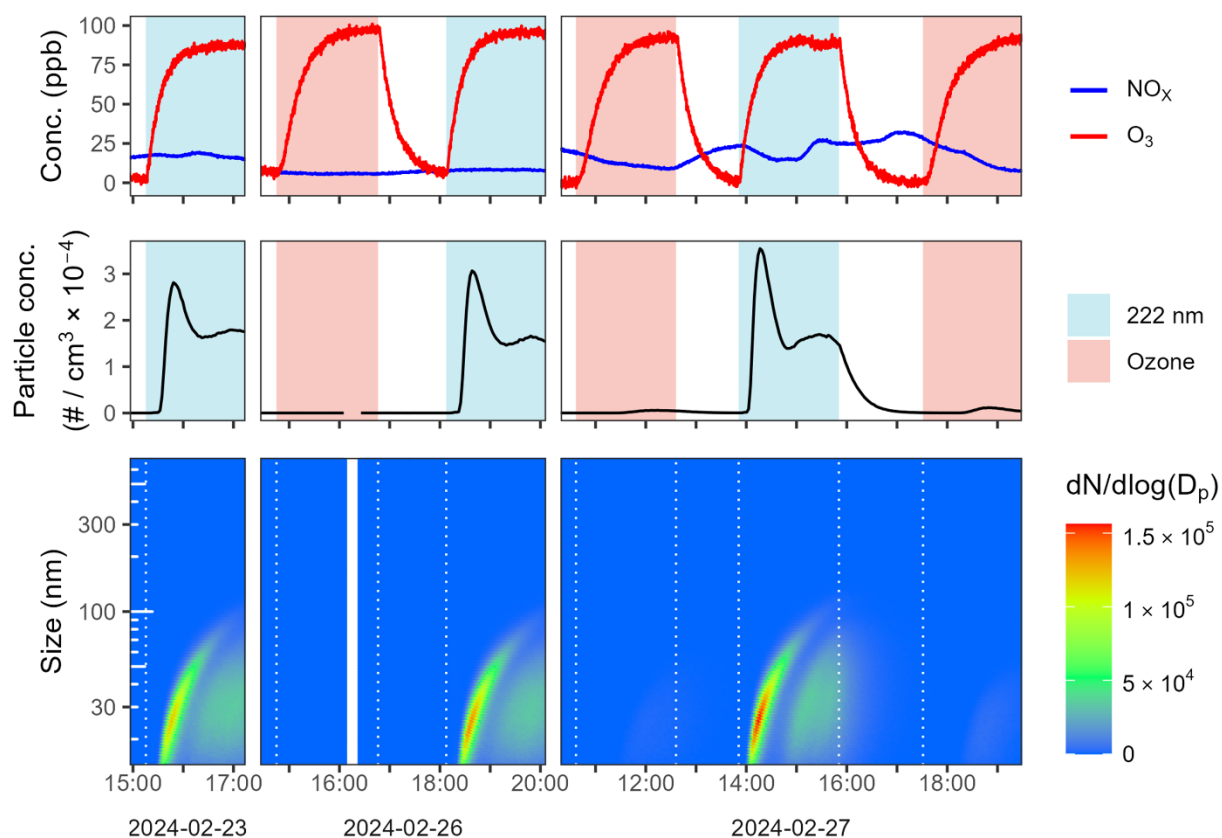


192
 193 *Figure 1: New particle formation from limonene + GUV₂₂₂ vs limonene + O₃. Panel A: particle*
 194 *growth and new particle formation for two example experiments (expt. 22 and 23). The top*
 195 *panels show O₃ and limonene concentrations, the middle panels show total particle number*
 196 *concentration over time, and the bottom panels show number-weighted size distributions over*
 197 *time. The spikes in particle concentration before t = 0 correspond to the addition of ammonium*
 198 *sulfate seed particles. Similar plots for all experiments are shown in the SI. Panel B: maximum*
 199 *number concentration of nucleated particles for each experiment (circles), grouped by*
 200 *experimental condition. See supporting information for further details on the determination of*
 201 *these values.*

202 Such differences in new particle formation occur under every chemical condition tested
 203 in the mini chamber (see Fig. S4 – S5). Figure 1B shows the maximum nucleated particle
 204 concentration for each experiment, allowing comparison of new particle formation for GUV₂₂₂
 205 vs. ozone-only conditions across different humidity and NO_x levels. The most nucleation occurs
 206 under dry conditions, whereas the least occurs in the presence of NO_x. This is consistent with the
 207 total SOA mass concentrations in mini chamber experiments; SOA mass is generally higher
 208 under dry conditions, and lower in the presence of ~20 ppb NO (see SI), suggesting that this
 209 trend may simply be controlled here by differences in SOA yield. While the maximum nucleated
 210 particle count varies dramatically between chamber conditions, it is always substantially greater
 211 under GUV₂₂₂ conditions than in comparable ozone-only experiments.

212 We performed an additional set of experiments (expts. 35 – 40) on a more complex
 213 system by filling the mini chamber with ambient air sampled continuously from outside our
 214 building. As shown in Fig. 2, new particles are formed every time the GUV₂₂₂ lamp is turned on,

215 while new particle formation under ozone-only conditions is almost negligible. Particles formed
 216 in the presence of GUV_{222} light reach number concentrations as high as 3.5×10^4 particles cm^{-3} ,
 217 before the total particle number concentration drops due to coagulation. As the first nucleated
 218 mode continues to grow, a second smaller nucleation event occurs, leading to a relatively steady
 219 total particle number concentration after about one hour. In contrast, the interspersed ozone-only
 220 experiments demonstrate little obvious nucleation (max. 16 – 1100 particles cm^{-3}). Under
 221 GUV_{222} conditions, particles grow to sufficient size to be detected as organic aerosol in the AMS
 222 (See Fig. S6). While reaction conditions in these experiments are not identical—for example,
 223 NO_x concentrations (top panels) change somewhat due to fluctuations in ambient
 224 concentrations—this cannot explain the substantial differences in new particle formation
 225 between the GUV_{222} and O_3 -only experiments.



226
 227 *Figure 2: New particle formation for experiments using sampled outdoor air. Shown are O_3 and*
 228 *NO_x concentrations over time (top row), particle number concentration over time (second row),*
 229 *and number-weighted size distributions over time (bottom row) for six experiments in which*
 230 *outdoor air is introduced (expt. 35 – 40). Experiments were carried out on three separate days.*
 231 *Periods when the 222 nm lamp was turned on, and when the ozone generator was turned on, are*
 232 *highlighted in pale blue and pale red, respectively, in the top two rows.*

233 In addition to the chamber experiments with limonene or outdoor air, several blank mini
 234 chamber experiments are run in which no VOCs (limonene or ambient species) are added to the
 235 chamber (expt. 14, 33, 34) (See Fig. S7). As in prior work,⁸ new particle formation occurs under

236 222 nm light when the mini chamber is thoroughly flushed with air from our clean air generator
237 (2023 experiments). However, after the compressor for the clean air generator was replaced, such
238 nucleation under GUV₂₂₂ irradiation is not observed. Further, nucleation does not occur during
239 blank experiments run with ultra zero air from a cylinder. Thus it seems likely that oxidation of
240 trace VOCs from the older compressor causes the new particle formation in earlier blank
241 experiments. The older compressor is used only for experiments 1 – 14 and does not influence
242 the interpretation of the results presented here (since GUV₂₂₂ and ozone-only experiments are
243 always run under identical conditions for each experiment set). Experiments 8 – 13 (mini
244 chamber limonene oxidation) are replicated with ultra zero air (expts. 21 – 26); while these
245 experiments differ slightly due to faster particle wall loss and lower seed particle concentration,
246 they produce the same qualitative results (See Fig. S5).

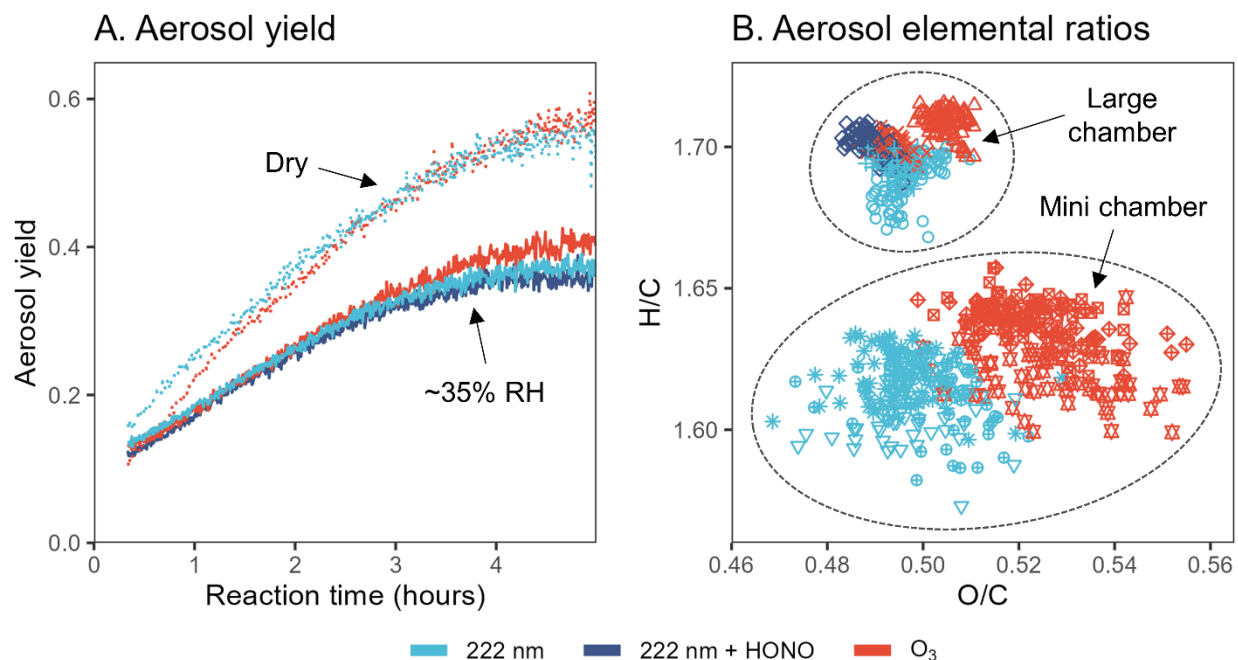
247 In marked contrast to mini chamber results, substantial new particle formation never
248 occurs in large chamber experiments (See Fig. S10 – S11). This is despite higher limonene
249 concentrations (and similar seed concentrations), which would be expected to slightly increase
250 new particle formation. However, a very small ($< \sim 200$ particles cm^{-3}) nucleation mode with
251 particles of diameter < 20 nm that do not grow in diameter forms consistently in both GUV₂₂₂
252 and ozone-only experiments when limonene is present (see Section S.5. in the supplement).
253 Based on the similarity of this mode between GUV₂₂₂ and ozone-only experiments, its formation
254 is likely an ozone-driven process.

255 The lack of substantial new particle formation in large chamber experiments may be
256 related to the reduced GUV₂₂₂ fluence rate ($< 10\%$ of that in the mini chamber). Similar to these
257 experiments, no nucleation was observed in the mini chamber in our previous work when the
258 GUV₂₂₂ lamp was attenuated by a factor of ~ 5 .⁸ These results suggest that new particle formation
259 may be nonlinear with respect to GUV₂₂₂ fluence rate, and imply that 222 nm fluence rates used
260 in indoor spaces, often a factor of ten or more lower than that used in the mini chamber, likely
261 will not drive the degree of new particle formation that was observed in this work.

262 *Aerosol yield and composition*

263 Given the differences in new particle formation, an additional set of limonene chamber
264 experiments were carried out to examine potential differences in aerosol yield and composition
265 between GUV₂₂₂ and ozone-only conditions. These were first investigated in five experiments in
266 the large chamber (expt. 3 – 7), since its lower surface-to-volume ratio enables better
267 quantification of aerosol formation. Figure 3A shows aerosol yield as a function of reaction time.
268 Aerosol yields under GUV₂₂₂ and ozone-only conditions are nearly identical, with the two
269 GUV₂₂₂ experiments featuring slightly lower yield by the end of the experiment. This slight
270 difference agrees with the subtle decrease in SOA formation rate in the presence of GUV₂₂₂
271 observed by Jenks et al.,⁹ and could be due to photolysis of SOA components, but may instead
272 simply be due to experimental variability. Relative humidity appears to play a far greater role,
273 with dry conditions increasing calculated yield by a factor as high as ~ 1.5 . The measured aerosol
274 yields fall within the large range of literature values for limonene oxidation (26 – 109%),^{25–28} but
275 trends in yield with respect to RH are different those reported previously where yield was found
276 to stay the same or even increase with increased humidity.^{9,27,29} When 9 – 18 ppb HONO is

277 added to one experiment, aerosol yield is not appreciably different from the yield measured
 278 under standard GUV_{222} conditions. While the causes for discrepancies between our
 279 measurements and previous measurements are unclear, these results clearly demonstrate that the
 280 differences in the GUV_{222} vs ozone-only experiments are small compared to other factors
 281 controlling the amount of SOA formed.



282
 283 *Figure 3. Aerosol yield and elemental composition from limonene oxidation under GUV_{222} and*
 284 *ozone-only conditions. Panel A: aerosol yield over time, calculated as mass concentration of*
 285 *SOA ($\mu\text{g m}^{-3}$) divided by mass concentration of limonene reacted ($\mu\text{g m}^{-3}$), for five large chamber*
 286 *experiments (expt. 3 – 7). Dotted lines show ~0% RH conditions while solid lines show results*
 287 *from ~35% RH experiments. Panel B: Van Krevelen diagram that shows elemental ratios*
 288 *obtained from high-resolution AMS analysis of experiments 3 – 7 and 8 – 13. Color refers to the*
 289 *oxidation conditions, while each point shape represents a different experiment. Points shown are*
 290 *for timepoints after the elemental composition has stabilized (from $t = 100$ to 300 min and $t = 15$*
 291 *to 50 min for large and mini chamber experiments, respectively). Note that the axes of Figure 3B*
 292 *are zoomed in substantially; the differences between experiment types, while repeatable, are*
 293 *quite small. See also Figure S14 for Van Krevelen diagrams from all experiments.*

294 Aerosol yields from the mini chamber experiments are not calculated given the large
 295 uncertainties arising from rapid wall loss. As in the large chamber experiments, uncorrected
 296 organic aerosol mass is higher under dry conditions when compared to directly comparable
 297 humid experiments. When NO_x is continuously added (with a steady-state level of ~18 ppb),
 298 organic aerosol mass is substantially depressed, but this does not differ between GUV_{222} and
 299 ozone-only conditions (See Fig. S13).

300 Figure 3B shows elemental ratios from high resolution AMS analysis of SOA, in both
 301 large chamber experiments (expt. 3 – 7) and the set of mini chamber experiments that featured

302 the greatest AMS organic signal (expt. 8 – 13) (results from all mini chamber experiments are
303 shown in Fig. S14). Points in Van Krevelen space are shown for timepoints after the elemental
304 composition has stabilized. All points fall within a relatively small range, but GUV₂₂₂-derived
305 aerosol features consistently lower O/C and H/C ratios than ozone-only experiments. While this
306 effect is less clear for the large chamber experiments, the difference between GUV₂₂₂ and ozone-
307 only O/C ratios in the mini chamber is statistically significant for the set of mini chamber
308 experiments shown ($p = 0.002$), likely due to the higher GUV₂₂₂ fluence rates. These differences
309 are also observed in other sets of mini chamber experiments (Fig. S14), but the difference is not
310 quite as clear, likely due to the lower AMS aerosol signal and poorer AMS peak-shape tuning.
311 While differences between GUV₂₂₂ and ozone-only elemental ratios are reproducible, they are
312 small in magnitude, and similar in magnitude to the differences induced by using different
313 chambers or different experimental conditions.

314 Discussion

315 Chamber experiments examining the oxidation of limonene under GUV₂₂₂ and ozone-
316 only conditions demonstrate relatively little difference in SOA yield and composition. The
317 differences observed between GUV₂₂₂ and ozone-only experiments, while reproducible, are often
318 similar or smaller in magnitude to the magnitude of differences induced by changes in other
319 experimental parameters (e.g., NO_x, RH, chamber type). This leads us to conclude that most of
320 the observed chemistry is driven by reactions with O₃, in agreement with findings by Jenks et al.⁹
321 However, one major difference is new particle formation, which is consistently much greater in
322 the presence of high-fluence rate 222 nm light in the mini chamber.

323 New particle formation from the oxidation of organic species is likely to proceed through
324 the formation of low volatility organic compounds. These may include high-mass species such as
325 highly oxidized molecules (HOMs)³⁰ or larger compounds with a large number of carbon atoms.
326 However, NH₄⁺ CIMS measurements (which were taken for only two sets of experiments; see
327 SI) show no clear differences in any high mass ions between GUV₂₂₂ and O₃-only conditions.
328 Likewise, the AMS provides no evidence of dramatically differing chemical composition of the
329 organic aerosol, with aerosol produced under GUV₂₂₂ conditions actually appearing to be slightly
330 less oxidized (Figure 3), suggesting that HOM formation is not responsible for differences in
331 nucleation. It is possible that even without the formation of HOMs, direct photoionization of
332 organic molecules could influence nucleation,³¹ but the energy of 222 nm photons at 222 nm (5.6
333 eV) is well below the threshold of ~8 eV for the most easily ionizable organic molecules. This
334 process would therefore require photons with wavelengths substantially shorter than 222 nm,
335 likely minimal based on published spectra,³ and ionization due to the simultaneous absorption of
336 two photons is highly unlikely given the low photon fluxes.

337 Other plausible causes for the differences in new particle formation include subtle
338 differences in reaction conditions. Nucleation may be strongly dependent on initial chamber
339 conditions, but these experiments do not feature systematic differences in ozone, seed particle, or
340 limonene concentration (see Figures S2 – S4). The photolysis of ozone by GUV₂₂₂ has been
341 identified as an additional source of OH in previous studies,^{6,8} which could potentially impact
342 new particle formation. However, mechanistic modeling using the Master Chemical

343 Mechanism³² run in F0AM,³³ suggests only modest increases in mean OH under GUV₂₂₂
344 conditions compared to ozone-only conditions (1.7×10^6 vs 1.4×10^6 molec cm⁻³) (see SI).
345 Modeled OH concentrations are also almost identical in the first few minutes of the experiment
346 when nucleation occurs, suggesting that this difference is unlikely to explain new particle
347 formation. This is further supported by AMS measurements: literature chamber studies suggest
348 that aerosol from the OH oxidation of monoterpenes features a substantially higher H/C ratio
349 than aerosol from ozonolysis,^{34,35} but our measurements consistently show a slightly lower H/C
350 ratio under GUV₂₂₂, suggesting that OH oxidation is unlikely to be the primary driver of aerosol
351 formation. Differences could also be explained by changes in radical chemistry due to the
352 photolysis of trace NO_Y species. However, the addition of NO_X in expts. 27 – 32 suppresses
353 nucleation relative to experiments with no added NO_X (Fig. 1); similarly, the addition of HONO
354 to a large chamber experiment does not impact nucleation or aerosol yield (Fig. 3). This is
355 contrary to our earlier speculation that NO_Y photolysis at 222 nm may have a major impact on
356 oxidant formation and secondary pollutant formation.⁸ The lack of any observed effect is likely a
357 result of the relatively low photon flux of the GUV₂₂₂ lights, which leads to photolysis rates that
358 are substantially slower than dilution ($j_{\text{NO}_2} = 2.0 \times 10^{-5}$ s⁻¹ in the mini chamber; $j_{\text{HONO}} = 9.2 \times 10^{-6}$
359 s⁻¹ in the large chamber; see the Supporting Information). Finally, differences in other trace
360 species such as HO₂ or RO₂ could also influence oxidation chemistry, but box modeling suggests
361 that concentrations of these do not differ appreciably (see SI).

362 While our measurements do not pinpoint a mechanistic cause of increased new particle
363 formation under GUV₂₂₂ conditions, they clearly identify several patterns. First, indirect or direct
364 photolytic processes are involved, since all variables except for light are held constant. Second,
365 new particle formation likely involves gas-phase organic compounds, since it only occurs when
366 VOCs are present (limonene, trace organics from clean air compressor, sampled ambient air).
367 The process is unlikely to involve organic species from chamber surfaces, since no nucleation is
368 observed in an ultra zero air blank experiment. The concentrations of such organic precursors
369 may be so low that they may be difficult to detect. For example, assuming the nucleated particles
370 (diameter < 20 nm) are organic, with O/C = 0.25, H/C = 2, and density = 1 g cm⁻³, even at their
371 highest observed volume concentrations they would account for no more than 0.2 ppb C.
372 Detection and characterization of such precursors might be possible via analytical techniques
373 aimed at detection of low-volatility species, such as nitrate chemical ionization mass
374 spectrometry³⁶ to measure HOMs, or atmospheric pressure interface mass spectrometry,³⁷ to
375 detect ambient ions and charged clusters.

376 Conclusion

377 This series of laboratory experiments demonstrates that most aspects of SOA formation
378 (e.g., yield, elemental composition, dependence on RH and NO_X) in the presence of GUV₂₂₂ are
379 consistent with ozonolysis chemistry. While some measured parameters such as the aerosol O/C
380 ratio vary reproducibly with respect to GUV₂₂₂ vs ozone-only conditions, the magnitude of these
381 differences is generally small in comparison to the changes induced by different experimental
382 conditions.

383 However, the major exception to this finding is the occurrence of new particle formation
384 in the presence of high levels of GUV_{222} . While the reason for this is not clear, substantial new
385 particle formation events in the presence of limonene, as well as in outdoor air pumped into the
386 chamber, are cause for concern for indoor applications due to the relatively high concentrations
387 of ultrafine particles formed. In real indoor environments, the risk of new particle formation may
388 be reduced, due to lower average GUV_{222} fluence rates and ubiquity of surfaces that may
389 encourage deposition,³⁸ but locally high fluence rates near a GUV_{222} lamp might still encourage
390 new particle formation or interact with surface reservoirs of semivolatile compounds in uncertain
391 ways. Indeed, recent work has detected new particle formation from GUV_{222} irradiation in a real
392 indoor space.¹¹ Still, further work is required to fully understand this process, particularly with
393 regard to the quantification of new particle formation as a function of 222 nm fluence rate and
394 VOC identity.

395 For the purposes of deploying GUV_{222} lamps in indoor spaces, these results provide
396 confirmation that most (though not all) observed chemistry follows that expected simply from
397 reaction with ozone, consistent with earlier work.⁹ While ozone has serious potential as an indoor
398 air pollutant,¹⁴ its chemistry is reasonably well understood. Our results suggest that indoor spaces
399 with GUV_{222} lamps may likely be reasonably well-represented in models simply by including the
400 lamps as an additional source of ozone, and ensuring that all downstream ozone chemistry (e.g.,
401 formation of OH, OVOCs, and SOA) is represented. Still, additional uncertainties remain,
402 including the influence of 222 nm light on indoor surfaces and surface-bound organic species, as
403 well as the cause of GUV_{222} -driven new particle formation. In addition to GUV_{222} -driven ozone
404 production, the new particle formation observed in this work represents a further reason to keep
405 GUV_{222} light intensity to the lowest effective levels when used in indoor spaces.

406

407 **Author contributions:**

408 MBG collected and analyzed the data and wrote the paper. JHK aided in project design, data
409 interpretation, and manuscript preparation.

410

411 **Acknowledgements:**

412 The authors thank Frank Keutsch and Yaowei Li (Harvard University) for the use of the NH_4^+
413 CIMS, and Victoria Barber (University of California, Los Angeles) for useful discussions. Data
414 are available on the Kroll Group publication website at
415 <http://krollgroup.mit.edu/publications.html>.

416

417 **Financial Support:**

418 This research has been supported by the Training Grant in Environmental Toxicology (MIT
419 Center for Environmental Health Sciences), and the MathWorks Engineering Fellowship Fund.

420 **References**

- 421 1 D. Welch, M. Buonanno, V. Grilj, I. Shuryak, C. Crickmore, A. W. Bigelow, G. Randers-
 422 Pehrson, G. W. Johnson and D. J. Brenner, Far-UVC light: A new tool to control the spread of
 423 airborne-mediated microbial diseases, *Sci. Rep.*, 2018, **8**, 2752.
- 424 2 M. Buonanno, D. Welch, I. Shuryak and D. J. Brenner, Far-UVC light (222 nm) efficiently
 425 and safely inactivates airborne human coronaviruses, *Sci. Rep.*, 2020, **10**, 10285.
- 426 3 M. Buonanno, D. Welch and D. J. Brenner, Exposure of Human Skin Models to KrCl Excimer
 427 Lamps: The Impact of Optical Filtering, *Photochem. Photobiol.*, 2021, **97**, 517–523.
- 428 4 K. Sugihara, S. Kaidzu, M. Sasaki, S. Ichioka, Y. Takayanagi, H. Shimizu, I. Sano, K. Hara
 429 and M. Tanito, One-year Ocular Safety Observation of Workers and Estimations of
 430 Microorganism Inactivation Efficacy in the Room Irradiated with 222-nm Far Ultraviolet-C
 431 Lamps, *Photochem. Photobiol.*, 2023, **99**, 967–974.
- 432 5 M. F. Link, A. Shore, B. H. Hamadani and D. Poppendieck, Ozone Generation from a
 433 Germicidal Ultraviolet Lamp with Peak Emission at 222 nm, *Environ. Sci. Technol. Lett.*,
 434 2023, **10**, 675–679.
- 435 6 Z. Peng, S. L. Miller and J. L. Jimenez, Model Evaluation of Secondary Chemistry due to
 436 Disinfection of Indoor Air with Germicidal Ultraviolet Lamps, *Environ. Sci. Technol. Lett.*,
 437 2023, **10**, 6–13.
- 438 7 Z. Peng, D. A. Day, G. A. Symonds, O. J. Jenks, H. Stark, A. V. Handschy, J. A. De Gouw and
 439 J. L. Jimenez, Significant Production of Ozone from Germicidal UV Lights at 222 nm,
 440 *Environ. Sci. Technol. Lett.*, 2023, **10**, 668–674.
- 441 8 V. P. Barber, M. B. Goss, L. J. Franco Deloya, L. N. LeMar, Y. Li, E. Helstrom, M.
 442 Canagaratna, F. N. Keutsch and J. H. Kroll, Indoor Air Quality Implications of Germicidal
 443 222 nm Light, *Environ. Sci. Technol.*, 2023, **57**, 15990–15998.
- 444 9 O. J. Jenks, Z. Peng, M. K. Schueneman, M. Rutherford, A. V. Handschy, D. A. Day, J. L.
 445 Jimenez and J. A. de Gouw, Effects of 222 nm Germicidal Ultraviolet Light on Aerosol and
 446 VOC Formation from Limonene, *ACS EST Air*, , DOI:10.1021/acsestair.4c00065.
- 447 10 Z. Liang, L. Zhou, K. Chen, Y.-H. Lin, Alvin. C. K. Lai, Patrick. K. H. Lee, Patrick. H. L. Sit,
 448 R. Yin and C. K. Chan, Formation of Secondary Aerosol by 222 nm Far-UVC Irradiation on
 449 SO₂, *Atmos. Environ.*, 2024, 120559.
- 450 11 M. Link, R. Robertson, A. Shore, B. Hamadani, C. Cecelski and D. Poppendieck, Ozone
 451 Generation and Chemistry from 222 nm Germicidal Ultraviolet Light in a Fragrant Restroom,
 452 *Environ. Sci. Process. Impacts*, , DOI:10.1039/D4EM00144C.
- 453 12 M. C. Turner, M. Jerrett, C. A. Pope, D. Krewski, S. M. Gapstur, W. R. Diver, B. S.
 454 Beckerman, J. D. Marshall, J. Su, D. L. Crouse and R. T. Burnett, Long-Term Ozone Exposure
 455 and Mortality in a Large Prospective Study, *Am. J. Respir. Crit. Care Med.*, 2016, **193**, 1134–
 456 1142.
- 457 13 E. Gakidou, A. Afshin, A. A. Abajobir, K. H. Abate, C. Abbafati, K. M. Abbas, F. Abd-Allah,
 458 A. M. Abdulle, S. F. Abera, V. Aboyans, L. J. Abu-Raddad, N. M. E. Abu-Rmeileh, G. Y.
 459 Abyu, I. A. Adedeji, O. Adetokunboh, M. Afarideh, A. Agrawal, S. Agrawal, H. Ahmadi, M.
 460 B. Ahmed, M. T. E. Aichour, A. N. Aichour, I. Aichour, R. O. Akinyemi, N. Akseer, F.
 461 Alahdab, Z. Al-Aly, K. Alam, N. Alam, T. Alam, D. Alasfoor, K. A. Alene, K. Ali, R.
 462 Alizadeh-Navaei, A. Alkerwi, F. Alla, P. Allebeck, R. Al-Raddadi, U. Alsharif, K. A.
 463 Altirkawi, N. Alvis-Guzman, A. T. Amare, E. Amini, W. Ammar, Y. A. Amoako, H. Ansari, J.
 464 M. Antó, C. A. T. Antonio, P. Anwari, N. Arian, J. Ärnlöv, A. Artaman, K. K. Aryal, H.
 465 Asayesh, S. W. Asgedom, T. M. Atey, L. Avila-Burgos, E. F. G. A. Avokpaho, A. Awasthi, P.

466 Azzopardi, U. Bacha, A. Badawi, K. Balakrishnan, S. H. Ballew, A. Barac, R. M. Barber, S. L.
467 Barker-Collo, T. Bärnighausen, S. Barquera, L. Barregard, L. H. Barrero, C. Batis, K. E.
468 Battle, B. R. Baumgarner, B. T. Baune, J. Beardsley, N. Bedi, E. Beghi, M. L. Bell, D. A.
469 Bennett, J. R. Bennett, I. M. Bensenor, A. Berhane, D. F. Berhe, E. Bernabé, B. D. Betsu, M.
470 Beuran, A. S. Beyene, A. Bhansali, Z. A. Bhutta, B. K. Bicer, B. Bikbov, C. Birungi, S.
471 Biryukov, C. D. Blosser, D. J. Boneya, I. R. Bou-Orm, M. Brauer, N. J. K. Breitborde, H.
472 Brenner, T. S. Brugha, L. N. B. Bulto, Z. A. Butt, L. Cahuana-Hurtado, R. Cárdenas, J. J.
473 Carrero, C. A. Castañeda-Orjuela, F. Catalá-López, K. Cercy, H.-Y. Chang, F. J. Charlson, O.
474 Chimed-Ochir, V. H. Chisumpa, A. A. Chitheer, H. Christensen, D. J. Christopher, M. Cirillo,
475 A. J. Cohen, H. Comfort, C. Cooper, J. Coresh, L. Cornaby, P. A. Cortesi, M. H. Criqui, J. A.
476 Crump, L. Dandona, R. Dandona, J. das Neves, G. Davey, D. V. Davitoiu, K. Davletov, B. de
477 Courten, B. K. Defo, L. Degenhardt, S. Deiparine, R. P. Dellavalle, K. Deribe, A. Deshpande,
478 S. D. Dharmaratne, E. L. Ding, S. Djalalinia, H. P. Do, K. Dokova, D. T. Doku, A. van
479 Donkelaar, E. R. Dorsey, T. R. Driscoll, M. Dubey, B. B. Duncan, S. Duncan, H. Ebrahimi, Z.
480 Z. El-Khatib, A. Enayati, A. Y. Endries, S. P. Ermakov, H. E. Erskine, B. Eshrati, S.
481 Eskandarieh, A. Esteghamati, K. Estep, E. J. A. Faraon, C. S. e S. Farinha, A. Faro, F.
482 Farzadfar, K. Fay, V. L. Feigin, S.-M. Fereshtehnejad, J. C. Fernandes, A. J. Ferrari, T. R.
483 Feyissa, I. Filip, F. Fischer, C. Fitzmaurice, A. D. Flaxman, N. Foigt, K. J. Foreman, J. J.
484 Frostad, N. Fullman, T. Fürst, J. M. Furtado, M. Ganji, A. L. Garcia-Basteiro, T. T.
485 Gebrehiwot, J. M. Geleijnse, A. Geleto, B. L. Gemechu, H. A. Gesesew, P. W. Gething, A.
486 Ghajar, K. B. Gibney, P. S. Gill, R. F. Gillum, A. Z. Giref, M. D. Gishu, G. Giussani, W. W.
487 Godwin, P. N. Gona, A. Goodridge, S. V. Gopalani, Y. Goryakin, A. C. Goulart, N. Graetz, H.
488 C. Gugnani, J. Guo, R. Gupta, T. Gupta, V. Gupta, R. A. Gutiérrez, V. Hachinski, N. Hafezi-
489 Nejad, G. B. Hailu, R. R. Hamadeh, S. Hamidi, M. Hammami, A. J. Handal, G. J. Hankey, S.
490 W. Hanson, H. L. Harb, H. A. Hareri, M. S. Hassanvand, R. Havmoeller, C. Hawley, S. I. Hay,
491 M. T. Hedayati, D. Hendrie, I. B. Heredia-Pi, J. C. M. Hernandez, H. W. Hoek, N. Horita, H.
492 D. Hosgood, S. Hostiuc, D. G. Hoy, M. Hsairi, G. Hu, J. J. Huang, H. Huang, N. M. Ibrahim,
493 K. M. Iburg, C. Ikeda, M. Inoue, C. M. S. Irvine, M. D. Jackson, K. H. Jacobsen, N.
494 Jahanmehr, M. B. Jakovljevic, A. Jauregui, M. Javanbakht, P. Jeemon, L. R. K. Johansson, C.
495 O. Johnson, J. B. Jonas, M. Jürisson, Z. Kabir, R. Kadel, A. Kahsay, R. Kamal, A. Karch, C.
496 K. Karema, A. Kasaeian, N. J. Kassebaum, A. Kastor, S. V. Katikireddi, N. Kawakami, P. N.
497 Keiyoro, S. G. Kelbore, L. Kemmer, A. P. Kengne, C. N. Kesavachandran, Y. S. Khader, I. A.
498 Khalil, E. A. Khan, Y.-H. Khang, A. Khosravi, J. Khubchandani, A. A. Kiadaliri, C. Kieling, J.
499 Y. Kim, Y. J. Kim, D. Kim, R. W. Kimokoti, Y. Kinfu, A. Kisa, K. A. Kissimova-Skarbek, M.
500 Kivimaki, L. D. Knibbs, A. K. Knudsen, J. A. Kopec, S. Kosen, P. A. Koul, A. Koyanagi, M.
501 Kravchenko, K. J. Krohn, H. Kromhout, G. A. Kumar, M. Kutz, H. H. Kyu, D. K. Lal, R.
502 Laloo, T. Lallukka, Q. Lan, V. C. Lansingh, A. Larsson, P. H. Lee, A. Lee, J. Leigh, J. Leung,
503 M. Levi, T. S. Levy, Y. Li, Y. Li, X. Liang, M. L. Liben, S. Linn, P. Liu, R. Lodha, G.
504 Logroscino, K. J. Looker, A. D. Lopez, S. Lorkowski, P. A. Lotufo, R. Lozano, R. Lunevicius,
505 E. R. K. Macarayan, H. Magdy Abd El Razek, M. Magdy Abd El Razek, M. Majdan, R.
506 Majdzadeh, A. Majeed, R. Malekzadeh, R. Malhotra, D. C. Malta, A. A. Mamun, H.
507 Manguerra, L. G. Mantovani, C. C. Mapoma, R. V. Martin, J. Martinez-Raga, F. R. Martins-
508 Melo, M. R. Mathur, K. Matsushita, R. Matzopoulos, M. Mazidi, C. McAlinden, J. J.
509 McGrath, S. Mehata, M. M. Mehndiratta, T. Meier, Y. A. Melaku, P. Memiah, Z. A. Memish,
510 W. Mendoza, M. M. Mengesha, G. A. Mensah, G. B. M. Mensink, S. T. Mereta, T. J.
511 Meretoja, A. Meretoja, H. B. Mezgebe, R. Micha, A. Millear, T. R. Miller, S. Minnig, M.

512 Mirarefin, E. M. Mirrakhimov, A. Misganaw, S. R. Mishra, K. A. Mohammad, K. E.
513 Mohammed, S. Mohammed, M. B. V. Mohan, A. H. Mokdad, L. Monasta, M. Montico, M.
514 Moradi-Lakeh, P. Moraga, L. Morawska, S. D. Morrison, C. Mountjoy-Venning, U. O.
515 Mueller, E. C. Mullany, K. Muller, G. V. S. Murthy, K. I. Musa, M. Naghavi, A. Naheed, V.
516 Nangia, G. Natarajan, R. I. Negoi, I. Negoi, C. T. Nguyen, Q. L. Nguyen, T. H. Nguyen, G.
517 Nguyen, M. Nguyen, E. Nichols, D. N. A. Ningrum, M. Nomura, V. M. Nong, O. F. Norheim,
518 B. Norrving, J. J. N. Noubiap, C. M. Obermeyer, F. A. Ogbo, I.-H. Oh, O. Oladimeji, A. T.
519 Olagunju, T. O. Olagunju, P. R. Olivares, H. E. Olsen, B. O. Olusanya, J. O. Olusanya, J. N.
520 Opio, E. Oren, A. Ortiz, E. Ota, M. O. Owolabi, M. Pa, R. E. Pacella, A. Pana, B. K. Panda, S.
521 Panda-Jonas, J. D. Pandian, C. Papachristou, E.-K. Park, C. D. Parry, S. B. Patten, G. C.
522 Patton, D. M. Pereira, N. Perico, K. Pesudovs, M. Petzold, M. R. Phillips, J. D. Pillay, M. A.
523 Piradov, F. Pishgar, D. Plass, M. A. Pletcher, S. Polinder, S. Popova, R. G. Poulton, F.
524 Pourmalek, N. Prasad, C. Purcell, M. Qorbani, A. Radfar, A. Rafay, A. Rahimi-Movaghar, V.
525 Rahimi-Movaghar, M. H. U. Rahman, M. A. Rahman, M. Rahman, R. K. Rai, S. Rajsic, U.
526 Ram, S. Rawaf, C. D. Rehm, J. Rehm, R. C. Reiner, M. B. Reitsma, G. Remuzzi, A. M. N.
527 Renzaho, S. Resnikoff, L. M. Reynales-Shigematsu, S. Rezaei, A. L. Ribeiro, J. A. Rivera, K.
528 T. Roba, D. Rojas-Rueda, Y. Roman, R. Room, G. Roshandel, G. A. Roth, D. Rothenbacher,
529 E. Rubagotti, L. Rushton, N. Sadat, M. Safdarian, S. Safi, S. Safiri, R. Sahathevan, J. Salama,
530 J. A. Salomon, A. M. Samy, J. R. Sanabria, M. D. Sanchez-Niño, T. G. Sánchez-Pimienta, D.
531 Santomauro, I. S. Santos, M. M. Santric Milicevic, B. Sartorius, M. Satpathy, M. Sawhney, S.
532 Saxena, M. I. Schmidt, I. J. C. Schneider, A. E. Schutte, D. C. Schwebel, F. Schwendicke, S.
533 Seedat, S. G. Sepanlou, B. Serdar, E. E. Servan-Mori, G. Shaddick, A. Shaheen, S. Shahraz,
534 M. A. Shaikh, M. Shamsipour, M. Shamsizadeh, S. M. Shariful Islam, J. Sharma, R. Sharma,
535 J. She, J. Shen, P. Shi, K. Shibuya, C. Shields, M. S. Shiferaw, M. Shigematsu, M.-J. Shin, R.
536 Shiri, R. Shirkoohi, K. Shishani, H. Shoman, M. G. Shrimme, I. D. Sigfusdottir, D. A. S. Silva,
537 J. P. Silva, D. G. A. Silveira, J. A. Singh, V. Singh, D. N. Sinha, E. Skiadaresi, E. L. Slepak, D.
538 L. Smith, M. Smith, B. H. A. Sobaih, E. Sobngwi, S. Soneji, R. J. D. Sorensen, L. A. Sposato,
539 C. T. Sreeramareddy, V. Srinivasan, N. Steel, D. J. Stein, C. Steiner, S. Steinke, M. A. Stokes,
540 B. Strub, M. Subart, M. B. Sufiyan, R. A. Suliankatchi, P. J. Sur, S. Swaminathan, B. L.
541 Sykes, C. E. I. Szoeki, R. Tabarés-Seisdedos, S. K. Tadakamadla, K. Takahashi, J. S. Takala,
542 N. Tandon, M. Tanner, Y. L. Tarekegn, M. Tavakkoli, T. K. Tegegne, A. Tehrani-Banihashemi,
543 A. S. Terkawi, B. Tessema, J. Thakur, O. Thamsuwan, K. R. Thankappan, A. M. Theis, M. L.
544 Thomas, A. J. Thomson, A. G. Thrift, T. Tillmann, R. Tobe-Gai, M. Tobollik, M. C. Tollanes,
545 M. Tonelli, R. Topor-Madry, A. Torre, M. Tortajada, M. Touvier, B. X. Tran, T. Truelsen, K. B.
546 Tuem, E. M. Tuzcu, S. Tyrovolas, K. N. Ukwaja, C. J. Uneke, R. Updike, O. A. Uthman, J. F.
547 M. van Boven, S. Varughese, T. Vasankari, L. J. Veerman, V. Venkateswaran, N.
548 Venketasubramanian, F. S. Violante, S. K. Vladimirov, V. V. Vlassov, S. E. Vollset, T. Vos, F.
549 Wadilo, T. Wakayo, M. T. Wallin, Y.-P. Wang, S. Weichenthal, E. Weiderpass, R. G.
550 Weintraub, D. J. Weiss, A. Werdecker, R. Westerman, H. A. Whiteford, C. S. Wiysonge, B. G.
551 Woldeyes, C. D. A. Wolfe, R. Woodbrook, A. Workicho, D. Xavier, G. Xu, S. Yadgir, B.
552 Yakob, L. L. Yan, M. Yaseri, H. H. Yimam, P. Yip, N. Yonemoto, S.-J. Yoon, M. Yotebieng, M.
553 Z. Younis, Z. Zaidi, M. E. S. Zaki, L. Zavala-Arciniega, X. Zhang, S. R. M. Zimsen, B.
554 Zipkin, S. Zodpey, S. S. Lim and C. J. L. Murray, Global, regional, and national comparative
555 risk assessment of 84 behavioural, environmental and occupational, and metabolic risks or
556 clusters of risks, 1990–2016: a systematic analysis for the Global Burden of Disease Study
557 2016, *The Lancet*, 2017, **390**, 1345–1422.

- 558 14 W. W. Nazaroff and C. J. Weschler, Indoor ozone: Concentrations and influencing factors,
559 *Indoor Air*, DOI:10.1111/ina.12942.
- 560 15 C. J. Weschler and W. W. Nazaroff, Ozone Loss: A Surrogate for the Indoor Concentration of
561 Ozone-Derived Products, *Environ. Sci. Technol.*, 2023, **57**, 13569–13578.
- 562 16 M. F. Link, R. Robertson, M. S. Claflin and D. Poppendieck, Quantification of Byproduct
563 Formation from Portable Air Cleaners Using a Proposed Standard Test Method, *Environ. Sci.*
564 *Technol.*, DOI:10.1021/acs.est.3c09331.
- 565 17 B. K. Coleman, M. M. Lunden, H. Destailats and W. W. Nazaroff, Secondary organic aerosol
566 from ozone-initiated reactions with terpene-rich household products, *Atmos. Environ.*, 2008,
567 **42**, 8234–8245.
- 568 18 K. Lee, J. Xue, A. S. Geyh, H. Ozkaynak, B. P. Leaderer, C. J. Weschler and J. D. Spengler,
569 Nitrous acid, nitrogen dioxide, and ozone concentrations in residential environments.,
570 *Environ. Health Perspect.*, 2002, **110**, 145–150.
- 571 19 C. Wang, B. Bottorff, E. Reidy, C. M. F. Rosales, D. B. Collins, A. Novoselac, D. K. Farmer,
572 M. E. Vance, P. S. Stevens and J. P. D. Abbatt, Cooking, Bleach Cleaning, and Air
573 Conditioning Strongly Impact Levels of HONO in a House, *Environ. Sci. Technol.*, 2020, **54**,
574 13488–13497.
- 575 20 J. F. Hunter, A. J. Carrasquillo, K. E. Daumit and J. H. Kroll, Secondary Organic Aerosol
576 Formation from Acyclic, Monocyclic, and Polycyclic Alkanes, *Environ. Sci. Technol.*, 2014,
577 **48**, 10227–10234.
- 578 21 C. Y. Lim, D. H. Hagan, M. M. Coggon, A. R. Koss, K. Sekimoto, J. de Gouw, C. Warneke, C.
579 D. Cappa and J. H. Kroll, Secondary organic aerosol formation from the laboratory oxidation
580 of biomass burning emissions, *Atmospheric Chem. Phys.*, 2019, **19**, 12797–12809.
- 581 22 P. F. DeCarlo, J. R. Kimmel, A. Trimborn, M. J. Northway, J. T. Jayne, A. C. Aiken, M. Gonin,
582 K. Fuhrer, T. Horvath, K. S. Docherty, D. R. Worsnop and J. L. Jimenez, Field-Deployable,
583 High-Resolution, Time-of-Flight Aerosol Mass Spectrometer, *Anal. Chem.*, 2006, **78**, 8281–
584 8289.
- 585 23 M. R. Canagaratna, J. L. Jimenez, J. H. Kroll, Q. Chen, S. H. Kessler, P. Massoli, L.
586 Hildebrandt Ruiz, E. Fortner, L. R. Williams, K. R. Wilson, J. D. Surratt, N. M. Donahue, J. T.
587 Jayne and D. R. Worsnop, Elemental ratio measurements of organic compounds using aerosol
588 mass spectrometry: characterization, improved calibration, and implications, *Atmospheric*
589 *Chem. Phys.*, 2015, **15**, 253–272.
- 590 24 A. Zaytsev, M. Breitenlechner, A. R. Koss, C. Y. Lim, J. C. Rowe, J. H. Kroll and F. N.
591 Keutsch, Using collision-induced dissociation to constrain sensitivity of ammonia chemical
592 ionization mass spectrometry (NH₄⁺ CIMS) to oxygenated volatile organic compounds,
593 *Atmospheric Meas. Tech.*, 2019, **12**, 1861–1870.
- 594 25 S. Leungsakul, M. Jaoui and R. M. Kamens, Kinetic Mechanism for Predicting Secondary
595 Organic Aerosol Formation from the Reaction of d-Limonene with Ozone, *Environ. Sci.*
596 *Technol.*, 2005, **39**, 9583–9594.
- 597 26 J. Zhang, K. E. Huff Hartz, S. N. Pandis and N. M. Donahue, Secondary Organic Aerosol
598 Formation from Limonene Ozonolysis: Homogeneous and Heterogeneous Influences as a
599 Function of NO_x, *J. Phys. Chem. A*, 2006, **110**, 11053–11063.
- 600 27 H. Saathoff, R. Tillmann and U. Schurath, Temperature dependence of yields of secondary
601 organic aerosols from the ozonolysis of α -pinene and limonene, *Atmos Chem Phys*, 2009, **27**.

- 602 28X. Chen and P. K. Hopke, A chamber study of secondary organic aerosol formation by
603 limonene ozonolysis: Chamber study of secondary organic aerosol formation, *Indoor Air*,
604 2010, **20**, 320–328.
- 605 29Y. Gong and Z. Chen, Quantification of the role of stabilized Criegee intermediates in the
606 formation of aerosols in limonene ozonolysis, *Atmospheric Chem. Phys.*, 2021, **21**, 813–829.
- 607 30F. Bianchi, T. Kurtén, M. Riva, C. Mohr, M. P. Rissanen, P. Roldin, T. Berndt, J. D. Crouse,
608 P. O. Wennberg, T. F. Mentel, J. Wildt, H. Junninen, T. Jokinen, M. Kulmala, D. R. Worsnop,
609 J. A. Thornton, N. Donahue, H. G. Kjaergaard and M. Ehn, Highly Oxygenated Organic
610 Molecules (HOM) from Gas-Phase Autoxidation Involving Peroxy Radicals: A Key
611 Contributor to Atmospheric Aerosol, *Chem. Rev.*, 2019, **119**, 3472–3509.
- 612 31A. Hirsikko, T. Nieminen, S. Gagné, K. Lehtipalo, H. E. Manninen, M. Ehn, U. Hörrak, V.-M.
613 Kerminen, L. Laakso, P. H. McMurry, A. Mirme, S. Mirme, T. Petäjä, H. Tammet, V. Vakkari,
614 M. Vana and M. Kulmala, Atmospheric ions and nucleation: a review of observations,
615 *Atmospheric Chem. Phys.*, 2011, **11**, 767–798.
- 616 32S. M. Saunders, M. E. Jenkin, R. G. Derwent and M. J. Pilling, Protocol for the development
617 of the Master Chemical Mechanism, MCM v3 (Part A): tropospheric degradation of non-
618 aromatic volatile organic compounds, *Atmospheric Chem. Phys.*, 2003, **3**, 161–180.
- 619 33G. M. Wolfe, M. R. Marvin, S. J. Roberts, K. R. Travis and J. Liao, The Framework for 0-D
620 Atmospheric Modeling (F0AM) v3.1, *Geosci. Model Dev.*, 2016, **9**, 3309–3319.
- 621 34D. F. Zhao, M. Kaminski, P. Schlag, H. Fuchs, I.-H. Acir, B. Bohn, R. Häsel, A. Kiendler-
622 Scharr, F. Rohrer, R. Tillmann, M. J. Wang, R. Wegener, J. Wildt, A. Wahner and T. F. Mentel,
623 Secondary organic aerosol formation from hydroxyl radical oxidation and ozonolysis of
624 monoterpenes, *Atmospheric Chem. Phys.*, 2015, **15**, 991–1012.
- 625 35J. Liu, E. L. D'Ambro, B. H. Lee, S. Schobesberger, D. M. Bell, R. A. Zaveri, A. Zelenyuk, J.
626 A. Thornton and J. E. Shilling, Monoterpene Photooxidation in a Continuous-Flow Chamber:
627 SOA Yields and Impacts of Oxidants, NO_x, and VOC Precursors, *Environ. Sci. Technol.*,
628 2022, **56**, 12066–12076.
- 629 36T. Jokinen, M. Sipilä, H. Junninen, M. Ehn, G. Lönn, J. Hakala, T. Petäjä, R. L. I. Mauldin, M.
630 Kulmala and D. R. Worsnop, Atmospheric sulphuric acid and neutral cluster measurements
631 using CI-API-TOF, *Atmospheric Chem. Phys.*, 2012, **12**, 4117–4125.
- 632 37H. Junninen, M. Ehn, T. Petäjä, L. Luosujärvi, T. Kotiaho, R. Kostianen, U. Rohner, M.
633 Gonin, K. Fuhrer, M. Kulmala and D. R. Worsnop, A high-resolution mass spectrometer to
634 measure atmospheric ion composition, *Atmospheric Meas. Tech.*, 2010, **3**, 1039–1053.
- 635 38W. W. Nazaroff, Indoor particle dynamics, *Indoor Air*, 2004, **14**, 175–183.
- 636